The Astrophysical Journal Letters, 815:L7 (6pp), 2015 December 10 doi:10.1088/2041-8205/815/1/L7

EVOLUTIONARY CLIMATE TRACKS OF EARTH-LIKE PLANETS

S. Kadoya[1] and E. Tajika[2]
[1] Department of Earth and Planetary Science, The University of Tokyo, Kiban Bldg. 408, 5-1-5, Kashiwanoha, Kashiwa, Chiba, 277-8561, Japan; kadoya@astrobio.k.u-tokyo.ac.jp
[2] Department of Complexity Science and Engineering, The University of Tokyo, Kiban Bldg. 409, 5-1-5, Kashiwanoha, Kashiwa, Chiba, 277-8561, Japan; tajika@k.u-tokyo.ac.jp
Received 2015 September 6; accepted 2015 November 21; published 2015 December 3

ABSTRACT

Recent studies have revealed that, in addition to insolation, the CO_2 degassing rate is an important limiting factor on the resulting climate of Earth-like planets. The CO_2 degassing rate should change with time owing to the thermal evolution of planetary interiors. Here we use a mantle degassing model coupled with a parameterized convection model to estimate the climatic evolution of Earth-like planets with different masses and distances from their central stars. The CO_2 degassing rate decreases monotonically with time owing to the decreasing mantle temperature. The CO_2 degassing rate for large planets is higher than that for small planets because the interiors of large planets are hotter than those of small planets. However, the effects arising from the difference in CO_2 degassing rate could be compensated by the difference in the silicate weathering rate derived from the difference in the surface area among planets with different size and with a similar land/sea ratio as the Earth. These results indicate that most of the Earth-like planets in the outer regions of the habitable zones (HZs) of old planetary systems are in the "snowball" climate mode (i.e., oscillating between snowball and warm states), irrespective of planetary mass. Because the snowball state lasts much longer than the warm climate state, Earth-like planets in HZs around old stars would statistically be observed as "snowball planets."

Key words: planets and satellites: surfaces

1. INTRODUCTION

An Earth-like planet characterized by liquid water (H_2O) on its surface is called a habitable planet, because the presence of liquid water is thought to be a fundamental condition for the existence of life. Studies of the conditions pertaining to habitable planets have focused mainly on their insolation from their central stars. The orbital region that satisfies these conditions is defined as the habitable zone (HZ; e.g., Kasting et al. 1993; Kopparapu et al. 2013). Some greenhouse gases, such as carbon dioxide, water vapor, methane, or pressure-induced effects by hydrogen or nitrogen, are necessary for warming planets (e.g., Kasting et al. 1993; Stevenson 1999; Kopparapu et al. 2013). Carbon dioxide has been assumed to be a major greenhouse gas. Several bars of atmospheric CO_2 are necessary to warm planets orbiting near the outer boundary of the HZ (e.g., Kasting et al. 1993; Kopparapu et al. 2013).

On Earth, the atmospheric CO_2 level is thought to be controlled by the carbonate–silicate geochemical cycle (Walker et al. 1981). When liquid water, CO_2, and silicate rocks coexist, atmospheric CO_2 is consumed owing to the chemical weathering of silicate minerals, followed by precipitation of carbonate minerals. The rate of this process depends on the surface temperature. On the other hand, CO_2 is supplied to the atmosphere through volcanism, which is independent of surface temperature. Therefore, the carbonate–silicate geochemical cycle is a negative feedback mechanism ("Walker feedback") with respect to the surface temperature (Walker et al. 1981). Consequently, Earth-like planets undergoing the carbonate–silicate geochemical cycle and orbiting within their stars' HZ are assumed to have a warm climate and liquid water on their surface.

However, recent studies (Tajika 2003, 2007, 2008; Kadoya & Tajika 2014) have revealed that Earth-like planets in the HZ (even Earth itself) repeatedly become globally ice-covered if the rate of CO_2 degassing from the planetary interior is lower than a critical value, which depends on the insolation and other factors that affect silicate weathering. For example, when Earth-like planets characterized by a CO_2 degassing rate similar to that of the present-day Earth receive less than 0.9 times the present solar flux, they should be in the "snowball" climate mode (Kadoya & Tajika 2014). Such planets alternately experience a snowball state (completely globally ice-covered) and a warm state (liquid water occurs on the planetary surface). Such "snowball planets" would have internal oceans beneath their surface ice, and they are expected to exist both within and outside the HZ (Tajika 2008). However, for higher CO_2 degassing rates, planets could be in the warm climate mode, even when their insolation is <0.9 times the present solar flux on Earth (Kadoya & Tajika 2014). Hence, the rate of CO_2 degassing through volcanism is important in considering the climate mode of Earth-like planets.

The rate of CO_2 degassing through volcanism depends on an internal activity of the planet. Tajika & Matsui (1992, 1993) reconstructed the evolution of CO_2 atmosphere on the Earth by investigating the evolution of the CO_2 degassing rate, the carbonate–silicate geochemical cycle, and the resulting climate throughout the Earth's history based on a thermal evolution model of the mantle, coupled with a model of volatile exchange between the surface and the mantle. A similar model has also been used to reveal the duration of habitability of extrasolar planets, with a particular focus on the condition for photosynthetic organisms (Franck et al. 2001; von Bloh et al. 2007, 2009, 2011). The evolution of the CO_2 degassing rate may, therefore, constrain the climatic evolution of Earth-like planets.

In this paper, we examine the climatic evolution of Earth-like planets based on the evolution of the CO_2 degassing rate and their insolation. We show the evolutionary tracks of climate of Earth-like planets as a function of both time (age) and orbital

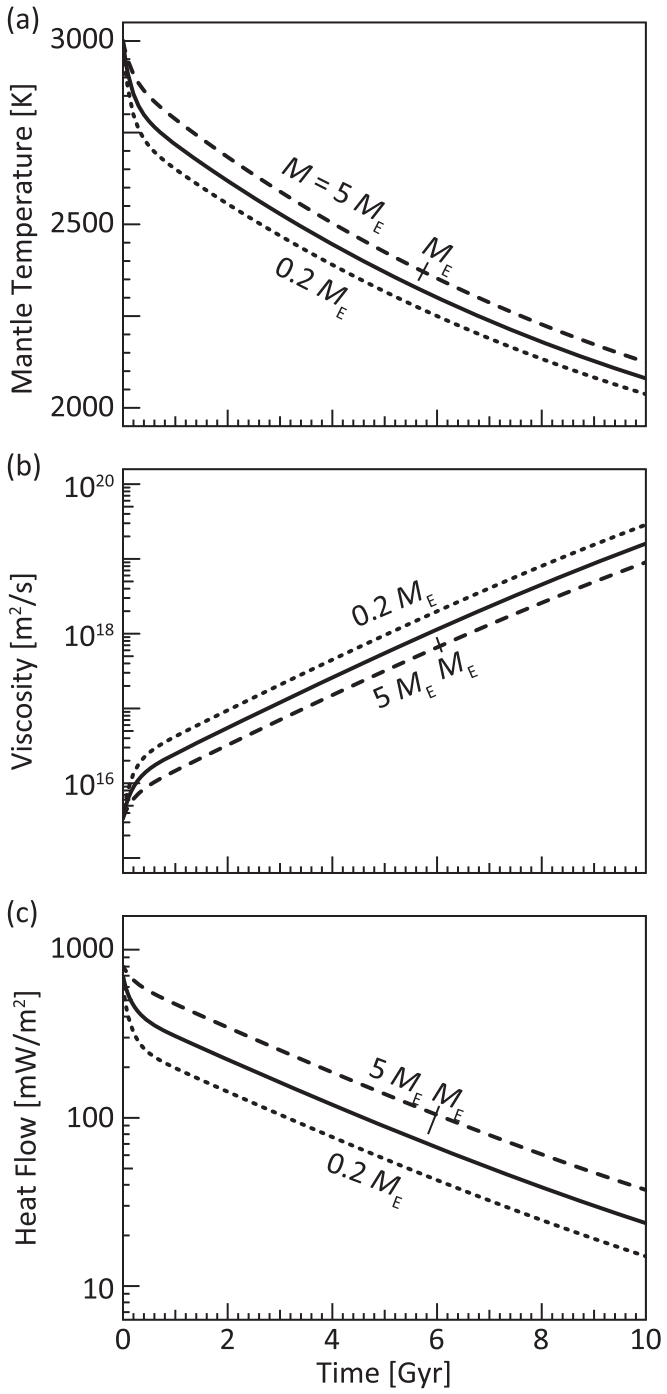

Figure 1. (a) Average mantle temperature, (b) mantle viscosity, and (c) heat flow from the mantle as a function of time. The solid line represents an Earth-mass planet. The dashed and dotted lines represent planets with masses that are five times larger and smaller than the Earth's mass, respectively. The decrease in mantle temperature results in higher viscosity and lower heat flow from the mantle.

semimajor axis, and we discuss the effect of the planetary mass on climatic evolution.

2. MODEL

We define an Earth-like planet as a terrestrial planet that has oceans, continents, and active plate tectonics. We assume an areal land fraction of 0.3, distributed latitudinally uniformly for simplicity.

The evolution of the mantle temperature is calculated using a parameterized convection model (e.g., Tajika & Matsui 1992) for different planetary masses (i.e., radii). The basic equation of the model is

$$C_{\rm m}\frac{dT_{\rm m}}{dt} = -\frac{3R_{\rm m}^2}{R_{\rm m}^3 - R_{\rm c}^3}q(T_{\rm m}) + Q(t), \quad (1)$$

where $T_{\rm m}$ is the average mantle temperature, t is the time coordinate, $C_{\rm m}$ is the heat capacity, $R_{\rm m}$ and $R_{\rm c}$ are the mantle and core radii, respectively, q represents the heat flow from the mantle, and Q is the energy production rate in the mantle. We adopt the scaling law of Valencia et al. (2006) to calculate the mantle and core radii from the planetary mass; i.e., $R_i = R_i^* \times (M/M_{\rm E})^{a_i}$, where i denotes "m" (mantle) or "c" (core), R_i^* is the radius of the mantle (core) of the Earth, and M and $M_{\rm E}$ are the planetary and Earth masses, respectively. The scaling exponents $a_{\rm m}$ and $a_{\rm c}$ are 0.27 and 0.247, respectively (Valencia et al. 2006).

The heat flow from the mantle, q, is parameterized as $q(T_{\rm m}) = k(T_{\rm m} - T_{\rm s})/(R_{\rm m} - R_{\rm c}) \times Nu(T_{\rm m})$, where k is the thermal conductivity and $T_{\rm s}$ the surface temperature. Because the variation in surface temperature is relatively small (200 K $< T_{\rm s} <$ 320 K) compared with that of the mantle temperature, the surface temperature is assumed to be constant at 273 K. The internal heat production rate in the mantle, Q, is calculated as $Q = Q_0 \exp(-\lambda t)$, where λ is average decay constant ($\equiv 3.4 \times 10^{-10}$ yr^{-1}).

The Nusselt number is calculated as $Nu(T_{\rm m}) = ({\rm Ra}(T_{\rm m})/{\rm Ra_c})^{1/3}$, where Ra is an internal Rayleigh number and $\rm Ra_c$ is the critical Rayleigh number ($\equiv 10^3$). The internal Rayleigh number is defined as ${\rm Ra}(T_{\rm m}) = \alpha g(T_{\rm m} - T_{\rm s})(R_{\rm m} - R_{\rm c})^3/\kappa\nu(T_{\rm m})$, where α is the thermal expansivity, g the gravitational acceleration, and κ the thermal diffusivity. The mantle viscosity, ν, is calculated as $\nu(T_{\rm m}) = \nu_0 \exp(A/RT_{\rm m})$, where A is the olivine activation energy and R is the gas constant.

In this study, active plate tectonics are assumed and the seafloor spreading rate, SR, is calculated as

$${\rm SR} = \frac{\pi\kappa S_{\rm o}}{\left\{2k\left(T_{\rm p} - T_{\rm s}\right)\right\}^2}q^2, \quad (2)$$

where $S_{\rm o}$ is area of ocean floor, and $T_{\rm p}$ is potential temperature of the mantle.

The melt generation depth, $d_{\rm m}$, is defined as the depth where the mantle temperature adiabatically intersects the solidus temperature of the upper mantle. The solidus temperature is calculated using a model fit to experimental results compiled by Hirschmann (2000).

The CO_2 degassing rate depends on the seafloor spreading rate, the melt generation depth, and the mantle carbon content (Tajika & Matsui 1992). However, because we assume that the mantle represents a much larger reservoir of carbon than the atmosphere and ocean combined (e.g., Sleep & Zhanle 2001), and that any change in the mantle carbon content would be small, the CO_2 degassing rate is calculated as

$$\frac{F_{\rm D}}{F_{\rm D}^*} = \frac{{\rm SR}d_{\rm m}}{{\rm SR}^* d_{\rm m}^*}, \quad (3)$$

where $F_{\rm D}$ is the CO_2 degassing rate, and $F_{\rm D}^*$, SR*, and d_m^* are the present values of the CO_2 degassing rate, the seafloor

spreading rate, and the melt generation depth, respectively. Hereafter, we refer to the product of the seafloor spreading rate and the melt generation depth as the melt generation volume.

The viscosity constant, ν_0, and the heat production constant, Q_0, are determined so that the mantle potential temperature and the mantle heat flow at $t = 4.6 \times 10^9$ years for the Earth-mass planet may be 1620 K and 100 mW m^{-2} (Turcotte & Schubert 2002; Herzberg et al. 2007). The other parameters are determined according to Tajika & Matsui (1992).

We adopt a climate-mode diagram obtained from a one-dimensional energy-balance climate model as a function of both an insolation and a CO_2 degassing rate (Kadoya & Tajika 2014). The rate of CO_2 uptake via silicate weathering depends on surface temperature, land area, runoff, existence of plant and so on (e.g., Berner 2006). In the model of Kadoya & Tajika (2014), however, the dependences on surface temperature and land area are considered for simplicity.

3. RESULTS AND DISCUSSION

Figure 1 shows the evolution of the average mantle temperature, the mantle viscosity, and the heat flow from the mantle. The solid lines represent the evolution of an Earth-mass planet. The dashed and dotted lines represent the evolution of planets whose masses are five times larger and smaller than the Earth's, respectively. The average mantle temperature decreases monotonically with time (see Figure 1(a)), which increases the mantle viscosity (see Figure 1(b)). The decrease in temperature, combined with the increase in viscosity, results in reduced heat flow from the mantle (see Figure 1(c)). As expected, the mantle temperatures of large planets remain higher than those of small planets. However, the difference in the average mantle temperature among planets of different masses is small (<100 K) because in small planets the higher viscosity caused by the lower mantle temperature results in a greater reduction in heat flow than in large planets. This finding is consistent with previous studies (Stevenson 2003; Kite et al. 2009; Schaefer & Sasselov 2015).

As the heat flow from the mantle decreases, the seafloor spreading rate also decreases monotonically (see Figure 2(a)). Since large planets have higher mantle temperatures (i.e., higher heat flows) than small planets (see Figure 1(c)), the seafloor spreading rate on large planets is higher than that on small planets (see Figure 1(a)). The melt generation depth also decreases monotonically with time (see Figure 2(b)), since the mantle temperature decreases (see Figure 1(a)). Because the gravitational acceleration is larger on large planets, the adiabatic temperature gradient is steeper (because $dT/dz = -g\alpha T/C_p$) than on small planets. Therefore, the melt generation depth is shallower on large planets than on small planets (see Figure 2(b)). However, the rapid decrease in the mantle temperature of small planets (see Figure 1(a)) results in a significant decrease in the melt generation depth during the late stages of their evolution (for ages >8 Gyr; see Figure 2(b)). Melt generation cannot occur at a mantle potential temperature below 1394 K (Hirschmann 2000), which corresponds to an age of ~10 Gyr for these planets. This timescale corresponds to the upper estimate to the timescale for CO_2 degassing owing to melting of mantle material. As a result, the melt generation volume ($=d_m \times SR$) decreases monotonically with time, and the volume for large planets is larger than that of Earth-sized planets by a factor of five on average, while the volume for small planets is smaller by a factor of three (see Figure 2(c)).

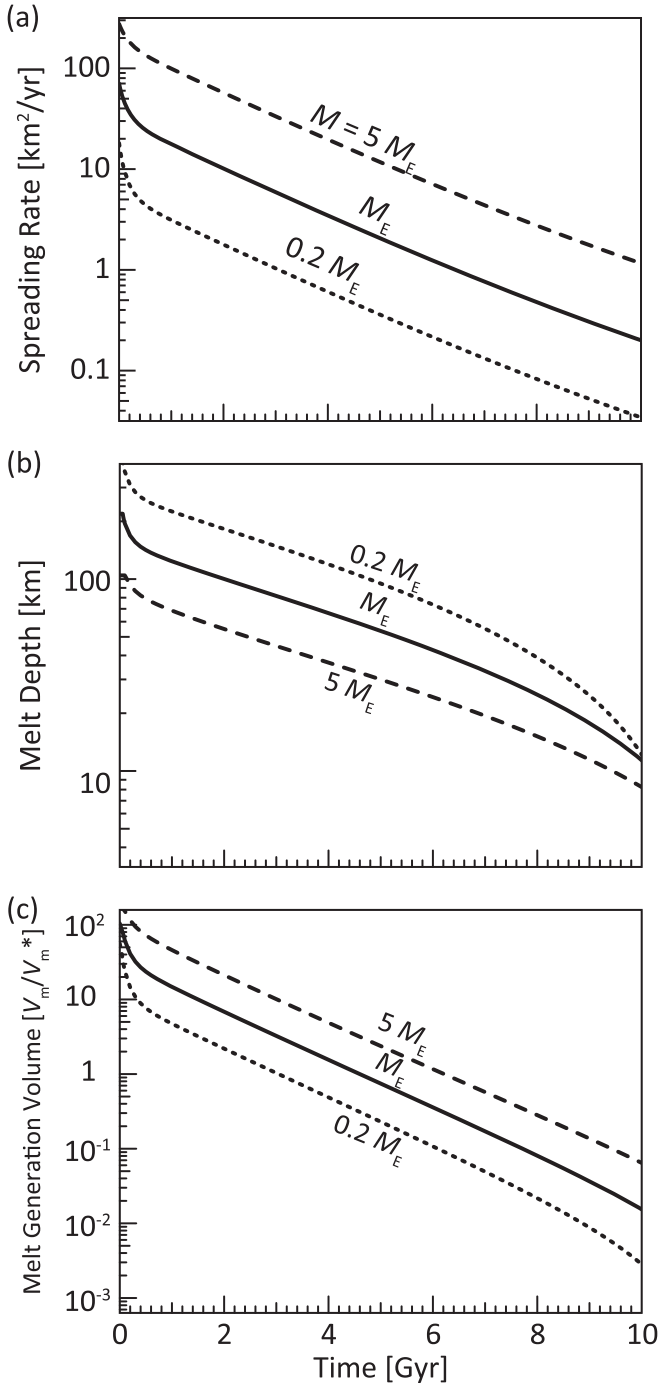

Figure 2. (a) Seafloor spreading rate, (b) melt generation depth, and (c) melt generation volume as a function of time. The solid line represents an Earth-mass planet. The dashed and dotted lines represent planets with masses that are five times larger and smaller than the Earth's, respectively. The decrease in mantle temperature and heat flow from the mantle (see Figure 1) result in decreases in the seafloor spreading rate, melt generation depth, and melt generation volume.

These results are consistent with those reported previously (Kite et al. 2009; Schaefer & Sasselov 2015).

Kadoya & Tajika (2014) estimated the climate mode under the condition where the planetary radiation balances the insolation, and the rate of CO_2 degassing through volcanism balances the rate of CO_2 uptake via silicate weathering for Earth-mass planets. The inner boundary of the HZ, which is

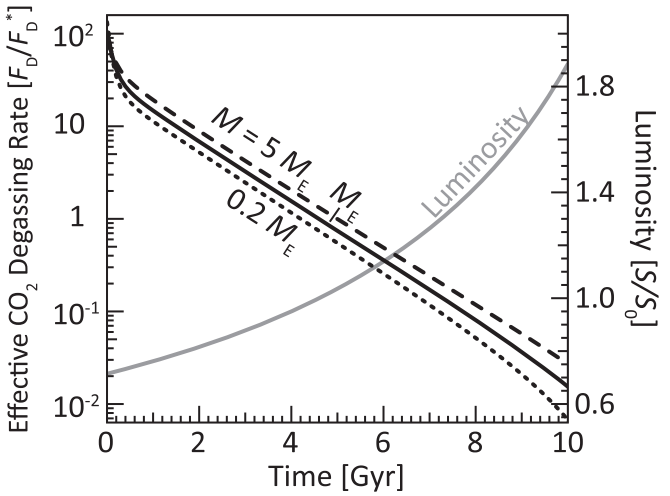

Figure 3. Effective CO_2 degassing rate and luminosity as a function of time. The CO_2 degassing rate has been corrected for the surface area of each planet. The luminosity is calculated using the model of Gough (1981). The differences in the effective CO_2 degassing rates for the different-mass planets are suppressed because of the differences in surface area.

controlled by the greenhouse effect of H_2O, depends on the planetary mass; i.e., the inner boundary for large planets is closer to the central star than that for small planets (Kopparapu et al. 2014). On the other hand, the outer boundary of the HZ, which is controlled by the greenhouse effect of CO_2, is largely independent of planetary mass because the greenhouse effect is largely compensated by the increasing planetary albedo (Kopparapu et al. 2014). Because we mainly focus on the outer region of the HZ, where the climate is controlled by the partial pressure of atmospheric CO_2 (pCO_2), the dependence on planetary mass of the HZ boundaries is not considered.

Planets of different masses also have different surface areas. For a given land/sea ratio, the land area that is subject to weathering should be larger for larger planets, and a correction to the CO_2 degassing rate is necessary to compare the evolution of the CO_2 degassing rate for different-mass planets when using the climate-mode diagram of Kadoya & Tajika (2014). Since the surface area is proportional to the square of the planetary radius, the "effective" CO_2 degassing rate, $F_{\rm D}^{\rm eff}$, is defined as

$$F_{\rm D}^{\rm eff} = \left(\frac{R_{\rm p}}{R_{\rm E}}\right)^{-2} F_{\rm D}, \quad (4)$$

where $R_{\rm p}$ is the planetary radius and $R_{\rm E}$ is the Earth's radius.

The effective CO_2 degassing rates for planets with different masses are shown in Figure 3. The correction given by Equation (4) reduces the difference in the CO_2 degassing rate for planets with different masses compared with the difference in the absolute CO_2 degassing rate (see Figure 2(c)). Note that planetary mass affects the operation and duration of plate tectonics; however, this problem is not discussed here because the impact of the planetary mass on plate tectonics is uncertain (e.g., Valencia et al. 2007; Korenaga 2010; Miyagoshi et al. 2014). Figure 3 also shows the luminosity evolution of the central star. We assume a G-type star (with the same mass as our Sun) as the central star and apply the model of luminosity evolution proposed by Gough (1981).

Figure 4(a) shows the climate diagram of Kadoya & Tajika (2014). The horizontal axis represents the solar flux, and the vertical axis is the effective CO_2 degassing rate. Both the horizontal and vertical axes are normalized to the values of present-day Earth. The climate of an Earth-like planet in the HZ

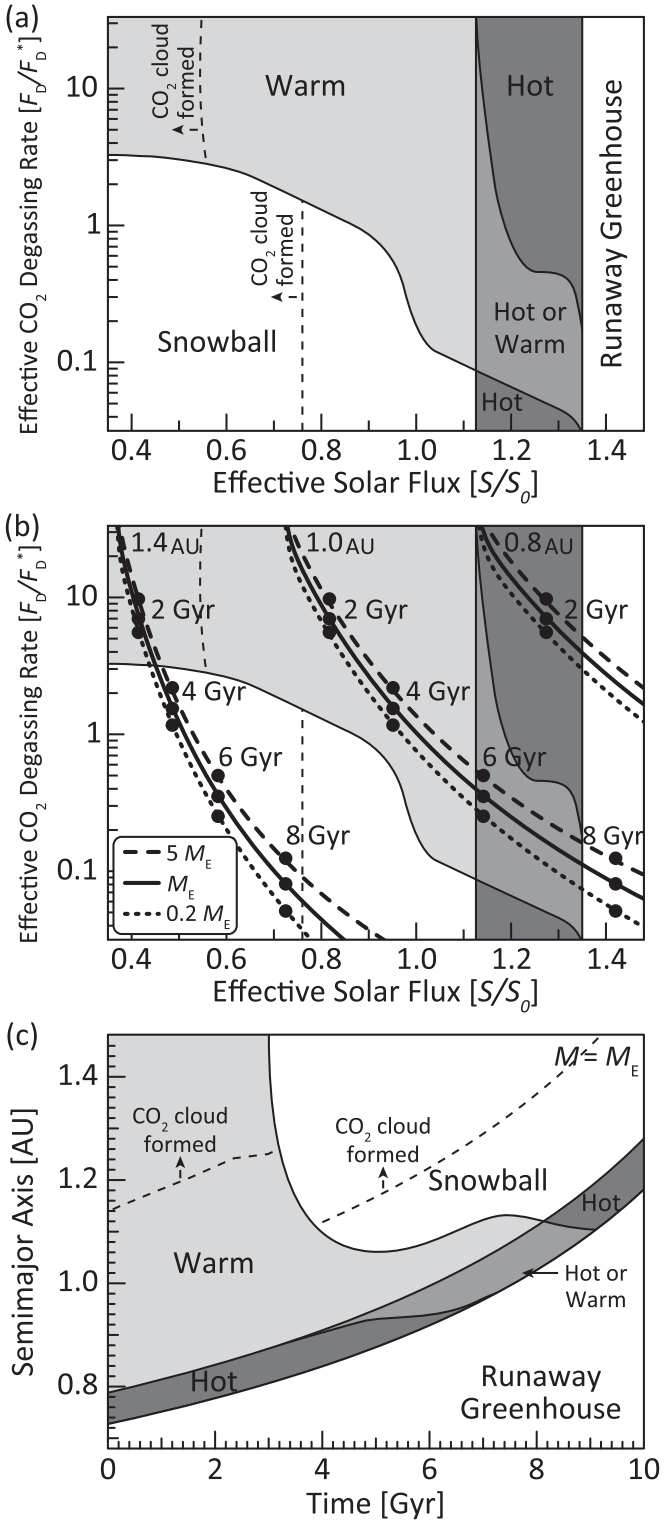

Figure 4. (a) Climate-mode diagram (Kadoya & Tajika 2014). (b) Evolution tracks in the climate-mode diagram. The dotted, solid, and dashed lines represent the evolution of planets with masses of 0.2, 1, and 5 $M_{\rm E}$ and that are located at 0.8, 1, and 1.4 AU from the central star, respectively. (c) Climate-mode evolution of an Earth-mass planet as a function of both time and orbital semimajor axis.

is classified into one of three climate modes: hot, warm, and snowball. In the warm climate mode, both energy and atmospheric CO_2 balances are achieved, and both the surface temperature and pCO_2 are controlled by Walker feedback. In the hot climate mode, which corresponds to moist greenhouse conditions (Kasting 1988), a planetary surface temperature is very high ($T_s > 400$ K), while pCO_2 is very low ($<10^{-7}$ bar). Although energy and atmospheric CO_2 balances are achieved, the carbonate–silicate geochemical cycle does not affect the surface temperature in this climate mode. In the snowball climate mode, neither the energy nor pCO_2 are balanced. Therefore, the climate is expected to oscillate between a snowball (globally ice-covered) state and a warm state (Tajika 2008; Kadoya & Tajika 2014; Menou 2015). When the effective solar flux is higher than a critical value, the planet enters a runaway greenhouse mode that makes the planet uninhabitable (for further discussion, see Kadoya & Tajika 2014).

The evolutionary climate tracks of planets with masses of 0.2, 1, and 5 M_E, and semimajor axes of 0.8, 1, and 1.4 AU are shown in Figure 4(b). Planets orbiting at 1 AU from their central star remain in warm climate mode for the first 6 Gyr and subsequently move into hot climate mode owing to the increase in luminosity as a result of stellar evolution. This is consistent with the previous result (Caldeira & Kasting 1992). Planets orbiting at 0.8 AU from their central star start in hot climate mode and then change to runaway greenhouse mode. For planets near their central star, the decrease in the CO_2 degassing rate does not have a meaningful effect on the evolution of the climate mode because the evolution of stellar luminosity plays a dominant role. On the other hand, planets orbiting at 1.4 AU from their central star possibly start in warm climate mode but change to snowball climate mode owing to the decrease in the CO_2 degassing rate within a few billion years. The timescale for changing to snowball climate mode depends on the planetary mass; i.e., planets with a mass five times smaller than the Earth's mass move into snowball climate mode 1 Gyr earlier than planets with a mass similar to that of the Earth.

The difference in the mass of the central star changes the timescale of luminosity evolution. Therefore, the evolutionary tracks of climate for the Earth-like planets around the star lighter than the Sun (e.g., an M-type star) are almost perpendicular to the horizontal axis in Figure 4(b), and the climate evolution is controlled solely by the evolution of CO_2 degassing rate.

Figure 4(c) again shows the evolution of the climate mode for planets with a mass of 1 M_E. The horizontal axis represents time, and the vertical axis represents the orbital semimajor axis. As discussed above, planets near their central star soon evolve to runaway greenhouse mode owing to stellar evolution. On the other hand, planets at great distances from their central star evolve to snowball climate mode owing to the decreasing CO_2 degassing rate. Planets orbiting at around 1.1 AU undergo a more complicated evolution: they start in warm climate mode, change snowball climate mode, return to warm climate mode, change to hot climate mode, and finally enter runaway greenhouse mode.

Planets at the outer boundary of the initial HZ around a G-type star are thought to remain in the HZ for more than a few billion years (Kasting et al. 1993). For example, planets orbiting at 1.4 AU (the maximum greenhouse limit of the initial HZ) remain in the HZ for 10 Gyr (Kasting et al. 1993). However, Figure 4(c) suggests that Earth-like planets at 1.4 AU go into snowball climate mode after 3 Gyr, although they are still located in the HZ. Kadoya & Tajika (2014) showed that although snowball climate-mode planets should oscillate between snowball and warm states, the snowball state lasts much longer than the warm state. Therefore, most Earth-like planets, at least those orbiting in the outer regions of the HZ of old planetary systems, will statistically tend to be observed as snowball planets. They may have internal oceans beneath their surface ice (Tajika 2008). It is noted that the decrease in the seafloor spreading rate may also affect an efficiency of CO_2 uptake through a decrease of tectonic activity, including mountain building which exposes fresh rocks to be weathered. However, there are many other factors which also affect an efficiency of CO_2 uptake, such as soil biological activity, vegetation, distribution of continents, coverage of basaltic rocks, and so on (e.g., Berner 2006). Here we just show a direct effect of the reduction of CO_2 degassing rate on climate evolution.

4. CONCLUSIONS

We examined the climatic evolution of Earth-like planets with masses of 0.2, 1, and 5 times the Earth's mass through the evolution of the CO_2 degassing rate of planets estimated using the parameterized convection model under the assumption of active plate tectonics. The seafloor spreading rate of large planets is higher than that of small planets owing to the higher average mantle temperature. On the other hand, the melt generation depth of large planets is shallower than that of small planets owing to the larger surface gravity of large planets. As a result, the net difference in the CO_2 degassing rates of large and small planets is relatively small. In addition, the difference in surface area of large and small planets compensates for the difference in the CO_2 degassing rate. As a result, large and small planets undergo a similar climatic evolution as long as plate tectonics are active (although the evolutionary timescale is 1 Gyr faster for planets with a mass five times smaller than the Earth's mass). The decrease in the effective CO_2 degassing rate with time results in planets orbiting in the outer regions of their HZ evolving to the snowball climate mode. Therefore, Earth-like planets in the HZ of old planetary systems are likely to be observed as snowball planets.

We would like to thank an anonymous reviewer for the reviews and helpful comments. This work was supported by a Grant-in-Aid for JSPS Fellows (No. 15J01965) from the Japan Society for the Promotion of Science.

REFERENCES

Berner, R. A. 2006, AmJS, 306, 295
Caldeira, K., & Kasting, J. F. 1992, Natur, 360, 721
Franck, S., von Bloh, W., Bounama, C., et al. 2001, AdSpR, 28, 695
Gough, D. O. 1981, SoPh, 74, 21
Herzberg, C., Asimow, P. D., Arndt, N., et al. 2007, GGG, 8, Q02006
Hirschmann, M. M. 2000, GGG, 1, 2000GC000070
Kadoya, S., & Tajika, E. 2014, ApJ, 790, 107
Kasting, J. F. 1988, Icar, 74, 472
Kasting, J. F., Whitmire, D. P., & Reynolds, R. T. 1993, Icar, 101, 108
Kite, E. S., Manga, M., & Gaidos, E. 2009, ApJ, 700, 1732
Kopparapu, R. K., Ramirez, R., Kasting, J. F., et al. 2013, ApJ, 765, 131
Kopparapu, R. K., Ramirez, R. M., SchottelKotte, J., et al. 2014, ApJL, 787, L29
Korenaga, J. 2010, JGRB, 115, B11405
McGovern, P. J., & Schubert, G. 1989, E&PSL, 96, 27

Menou, K. 2015, EPSL, 429, 20
Miyagoshi, T., Tachinami, C., Kameyama, M., & Ogawa, M. 2014, ApJL, 780, L8
Schaefer, L., & Sasselov, D. 2015, ApJ, 801, 40
Sleep, N. H., & Zhanle, K. 2001, JGR, 106, 1373
Stevenson, D. J. 1999, Natur, 400, 32
Stevenson, D. J. 2003, CRGeo, 335, 99
Tajika, E. 2003, E&PSL, 214, 443
Tajika, E. 2007, EP&S, 59, 293
Tajika, E. 2008, ApJL, 680, L53
Tajika, E., & Matsui, T. 1992, E&PSL, 113, 251
Tajika, E., & Matsui, T. 1993, GeoRL, 20, 851
Turcotte, D. L., & Schubert, G. 2002, Geodynamics (2nd ed.; New York: CUP)
Valencia, D., O'Connell, R. J., & Sasselov, D. 2006, Icar, 181, 545
Valencia, D., O'Connell, R. J., & Sasselov, D. D. 2007, ApJL, 670, L45
von Bloh, W., Bounama, C., Cuntz, M., & Franck, S. 2007, A&A, 476, 1365
von Bloh, W., Cuntz, M., Franck, S., & Bounama, C. 2011, A&A, 528, A133
von Bloh, W., Cuntz, M., Schröder, K.-P., et al. 2009, AsBio, 9, 593
Walker, J. C. G., Hays, P. B., & Kasting, J. F. 1981, JGR, 86, 9776